Size and Temperature Dependence of Electron Transfer between CdSe Quantum Dots and a TiO_2 Nanobelt

De Nyago Tafen[ab] and Oleg V. Prezhdo[c]

[a]National Energy Technology Laboratory, 1450 Queen Ave. SW, Albany, OR 97321, USA

[b]URS Corporation, P. O. Box 1959, Albany, OR 97321-0521, USA

[c]Department of Chemistry, University of Southern California, 3620 McClintock Avenue, Los Angeles, CA 90089, USA

ABSTRACT: Understanding charge transfer reactions between quantum dots (QD) and metal oxides is fundamental for improving photocatalytic, photovoltaic and electronic devices. The complexity of these processes makes it difficult to find an optimum QD size with rapid charge injection and low recombination. We combine time-domain density functional theory with nonadiabatic molecular dynamics to investigate the size and temperature dependence of the experimentally studied electron transfer and charge recombination at CdSe QD-TiO_2 nanobelt (NB) interfaces. The electron injection rate shows strong dependence on the QD size, increasing for small QDs. The rate exhibits Arrhenius temperature dependence, with the activation energy of the order of millielectronvolts. The charge recombination process occurs due to coupling of the electronic subsystem to vibrational modes of the TiO_2 NB. Inelastic electron-phonon scattering happens on a picosecond time scale, with strong dependence on the QD size. Our simulations demonstrate that the electron-hole recombination rate decreases significantly as the QD size increases, in excellent agreement with experiments. The temperature dependence of the charge recombination rates can be successfully modeled within the framework of the Marcus theory through optimization of the electronic coupling and the reorganization energy. Our simulations indicate that by varying the QD size, one can modulate the photoinduced charge separation and charge recombination, fundamental aspects of the design principles for high efficiency devices.

KEYWORDS: Nonadiabatic molecular dynamics; Time-domain density functional theory; Titanium dioxide; Quantum dots; Electron-phonon interaction; Electron transfer.

1. INTRODUCTION

Titanium dioxide (TiO_2) has established itself as one of the most widely used inorganic semiconductors in photocatalytic,[1-3] photovoltaic,[4-5] and photo-electrochemical[1] applications by virtue of its excellent physical and chemical stability, nontoxicity, desirable electronic and optical properties, and low cost. However, its photoactivity is limited partly by its large band gap (3.2 eV), allowing TiO_2 to absorb only ultraviolet light which is approximately 5% of the solar spectrum. Tremendous efforts have been made to enhance TiO_2 ability to harvest visible light. One way is through band gap narrowing by doping TiO_2 with impurity atoms such as nitrogen[6-7] or introducing defect states within the band gap. Yet, the large energy required to introduce dopant atoms restricts sample synthesis. An alternative approach is to couple TiO_2 with other materials such as molecular chromophores,[8-11] conjugated polymers,[12-14] nanoscale carbon materials,[15-16] and semiconductor quantum dots (QDs).[17-26]

Semiconductor QDs, such as CdSe with its tunable band gap, offer great opportunities to harvest light energy in the visible and infrared regions of solar spectrum. These small-band gap semiconductor nanostructures have unique ability to undergo efficient carrier multiplication under visible light photoexcitation.[27-28] In particular, they are capable to inject excited electrons and generate photocurrent under visible light irradiation when deposited on TiO_2 surfaces. The effect of size quantization allows one to tune the visible response and vary the band energies to modulate the charge transfer across different particle sizes.[18-19, 29] Robel *et al*. observed that as the size of the QD decreases, the small energy difference attained can increase the electron transfer (ET) rate by nearly 3 orders of magnitude.[19]

One-dimensional (1-D) TiO_2 nanomaterials, such as nanobelts, nanotubes and nanowires, have become a highly promising avenue in photocatalysis, solar cell and gas sensor technologies due to their confinement, and structurally well-defined physical and chemical properties. Although the energy gap of these single-crystalline 1-D nanostructures shows little alteration compared to the bulk TiO_2, they do display an increase in photoactivity due to better charge transport, higher surface defect content, and

larger surface area.[30-31] Wang *et al*. have shown that the use of TiO_2 nanobelts (NBs) instead of TiO_2 nanoparticles (NPs) not only permits a larger critical size of PbS QDs capable of injecting electrons into TiO_2 NBs, but also extends the effective absorption of the PbS-QD/TiO_2-NB nanohybrids to a longer wavelength region up to 1400 nm.[29] In our recent studies, we have characterized the photoinduced ET at CdSe-TiO_2 interfaces using real-time nonadiabatic molecular dynamics (NAMD) implemented within the time-dependent density functional theory (TD-DFT) framework[32-33] and have shown that the ET mechanism is non-adiabatic for the 1-D TiO_2 NB acceptor and adiabatic for the quasi 0-D TiO_2 NP.[17]

In view of the central importance of TiO_2 nanobelts and CdSe for technological applications, the current study uses the TD-DFT/NAMD approach to investigate the effect of the QD size on the interparticle ET process. The simulation shows that the interfacial ET in CdSe-QD/TiO_2-NB can be tuned through the size quantization effect of CdSe QDs, in agreement with the available experimental data.[19, 29] The present work also addresses the temperature dependence of the interfacial ET dynamics for charge separation and charge recombination.

This paper is organized as follows: The next section gives a brief summary of the theory underlying NAMD and TD-DFT, and describes the computational details. The results are discussed in section 3, which is separated into five parts focusing on the geometric and electronic structure of the Cd_nSe_n/TiO_2 interfaces, the vibrational motions contributing to the ET dynamics, the charge-separation dynamics, the electron-hole recombination dynamics, and the temperature effect on the interfacial ET dynamics. The simulation results are compared with the available experimental data. The Conclusions section summarizes the key findings of the current study.

2. THEORETICAL METHODOLOGIES

We use the mixed quantum-classical approach implementing the fewest switching surface hopping (FSSH) technique[34-35] within the time-dependent Kohn-Sham (KS) scheme to simulate the ET

dynamics.[32-33] In this approach, the electrons are treated quantum mechanically, while the nuclei are treated classically. The approach provides a detailed *ab initio* picture of the coupled electron-vibrational dynamics on the atomic scale and in the time-domain, and has proven to be efficient in many systems and processes.[8, 15, 17, 36-43]

A detailed description of the method can be found elsewhere.[44-46] The simulations are performed in the adiabatic representation, which are naturally produced by ab initio electronic structure theory. It should be noted that phenomenological, analytical models, such as the Marcus theory, employ diabatic representation. Diabatic states are usually defined to be localized on donor and acceptor species. Adiabatic states are eigenstates of the electronic Hamiltonian. They can change localization due to nuclear motions. Diabatic surfaces can cross in energy, while adiabatic surfaces instead undergo "avoided crossings" near the diabatic crossings.

Geometry optimization, electronic structure, and adiabatic MD calculations were carried out using the Vienna *ab initio* simulation package (VASP).[47] The electron exchange correlation effects were described by a generalized gradient approximation using the Perdew-Burke-Ernzerhof (PBE) functional.[48] The projected-augmented wave (PAW) approach was used to describe the interaction of the ionic cores with the valence electrons.

The simulation uses the stoichiometric anatase nanobelt with (101) surface termination, since it is the most stable among the low index surfaces of anatase TiO_2. The initial geometry was fully relaxed to the nearest minimum structure, and the resulting structure was used to model $CdSe/TiO_2$ heterostructures. The (101) NB surface has a stepped structure with exposed 5-fold and 6-fold coordinated Ti atoms, as well as 2-fold and 3-fold coordinated O atoms.

The initial structures of the CdSe QD were generated from bulk wurtzite. Three sizes are considered in our simulations: Cd_6Se_6, $Cd_{13}Se_{13}$ and $Cd_{36}Se_{36}$ with diameter of 0.50, 1.00, and 1.30 nm, respectively. Each QD was placed in a box with at least 16 Å of vacuum between neighboring QDs, and

they were relaxed to their minimum energy nuclear geometry, determined by convergence of the forces on all atoms to less than 0.03 eV/Å.

The QD-TiO_2 NB systems were constructed by placing the QD above the TiO_2 NB surface. Periodic boundary conditions in three dimensions were applied. In order to avoid spurious interactions between periodic images of the system, 16 Å of vacuum were added along both y and z-directions. The systems were fully relaxed to their minimum configuration at T= 0 K. After relaxing the geometries at 0 K, uniform velocity rescaling was used to bring the temperature of the CdSe-TiO_2 systems to 100 K. The simulations at 100K represent, approximately, ultrahigh vacuum conditions accessible experimentally. For instance, such conditions were used to study photo-induced ET from molecular chromophores to TiO_2 by Willig and co-workers.[49,50] Since the simulation contain no solvent and ligands, they best correspond to such experiments. After that, depending on the system size, 3.7 to 5.3 ps adiabatic MD simulations were performed in the microcanonical ensemble with a 1.5 fs atomic time-step.

The adiabatic energies and NA couplings were calculated for each step of the MD run, and the classical path approximation to FSSH was used.[45] The adiabatic MD trajectories were used to sample the initial conditions and to carry out the NAMD simulations. A minimum of 350 geometries were selected randomly from the 3.7 to 5.3 ps adiabatic MD trajectories as initial conditions for the NAMD, to simulate charge transfer from the CdSe QD to the TiO_2 NB and electron-hole recombination from the TiO_2 NB to the CdSe QD. The duration of each NAMD trajectory depended on the QD size and temperature. The minimum duration was 0.7 ps for charge separation and 2.2 ps for charge recombination. An electron was promoted to the orbital corresponding to the lowest energy excitation of CdSe, and its evolution was tracked by solving the time-dependent KS equations, which were propagated with the second-order differencing scheme[51] using a 10^{-3} fs time step.

3. RESULTS AND DISCUSSIONS

3.1 Geometric and electronic structure of the CdSe-QD/TiO_2-NB systems.

The geometry and separation of CdSe adsorbed on TiO_2 characterize the strength of the CdSe-TiO_2 interfacial interaction which plays a key role in the determination of the rates and mechanisms of the ET processes[52]. Figure 1 illustrates the optimized and finite-temperature geometries of the simulated CdSe-TiO_2 systems. Several possible orientations have been considered for the adsorption of CdSe QDs in order to locate the most stable structure. The top, middle, and bottom panels illustrate the TiO_2 NB interacting with Cd_6Se_6, $Cd_{13}Se_{13}$ and $Cd_{36}Se_{36}$ QDs, respectively. A comparison of the systems at 0 K and 100 K indicates that thermal fluctuations impact the system geometries. At 0 K, all three QDs are bound to TiO_2 and form covalent bonds. In the Cd_6Se_6-TiO_2 system, the QD is connected to the NB via a Cd-O covalent bond of length 2.49 Å. As temperature is raised from 0 to 100 K, the QD rotates along the z-axis and forms additional covalent bonds (2 Cd-O and 2 Se-Ti bonds) with the NB. The formation of these covalent bonds increases the chemical interaction between the donor and acceptor species. The length of these bonds in the sample MD geometry represented in Figure 1 are 2.31 and 2.38 Å for Cd-O, and 2.71 and 2.78 Å for Se-Ti.

In the case of $Cd_{13}Se_{13}$-TiO_2 and $Cd_{36}Se_{36}$-TiO_2 systems, the QD is bound to TiO_2 at 0 K through two Se-Ti bonds with bond lengths of 3.03 Å for $Cd_{13}Se_{13}$-TiO_2, and 2.95 and 3.00 Å for the $Cd_{36}Se_{36}$-TiO_2. As temperature increases to 100 K, the QD-NB interaction decreases significantly. As a result, the average separation between the QD and NB increases, the Se-Ti bonds break, and the donor-acceptor coupling strength decreases.

The conformations and bond distances at 100 K presented in Figure 1 refer to a sample MD geometry selected randomly. We have also generated averages for each CdSe-TiO_2 system by sampling over 360 nuclear configurations throughout the MD. The difference between the average geometries and the sample geometries represented in Figure 1 is small. For example, in the case of Cd_6Se_6-TiO_2, the CdSe QD in the average geometry is connected to the NB via two Cd-O and two Se-Ti bonds as in the

sample MD geometry. The calculated average bond lengths are 2.44 ± 0.10 and 2.33 ± 0.06 Å for Cd-O; and 2.81 ± 0.06 and 2.74 ± 0.12 Å for Se-Ti.

ET can occur directly during photon absorption, adiabatically by atomic motion over a transition state, and non-adiabatically by a quantum transition/tunneling between donor and acceptor states.[8] ET to the acceptor during the optical excitation constitutes the direct ET mechanism. When the distance between the donor and acceptor species increases, both direct and adiabatic ET stop. In that case, ET proceeds by the NA mechanism. If the donor and acceptor species are very far from each other, ET becomes extremely slow, while energy transfer can still take place, in particular, by the Förster mechanism.[53]

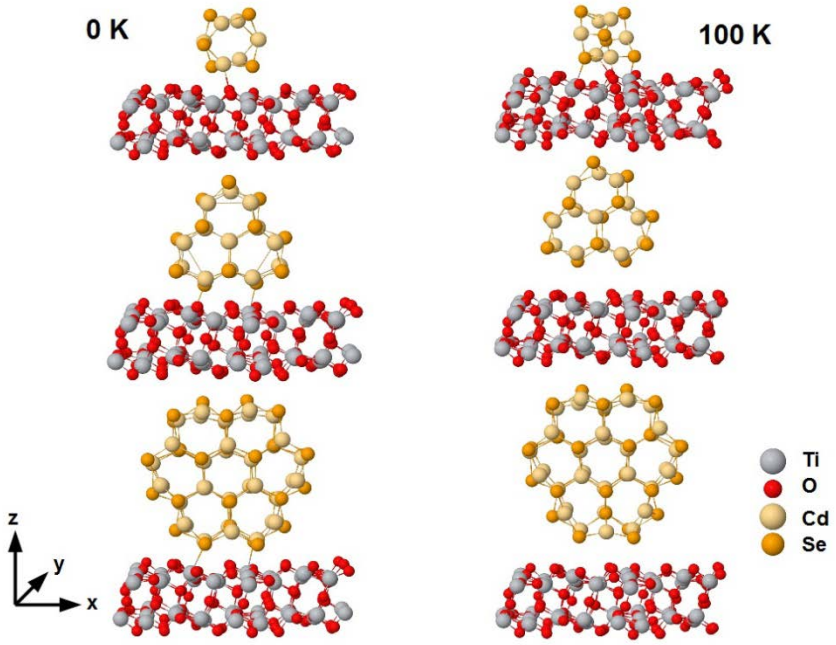

Figure 1. Side views of the CdSe-TiO_2 systems optimized at 0 K and during molecular dynamics at 100 K. Top: Cd_6Se_6-TiO_2 NB; middle: $Cd_{13}Se_{13}$-TiO_2 NB; bottom: $Cd_{36}Se_{36}$-TiO_2 NB. The geometry for 100 K is an MD snapshot.

Figure 2 shows the electronic density of states (DOS) of the combined system, separated into the contribution from Cd_nSe_n (red line) and the TiO_2 NB (black line). The change of the QD band gap due to

size quantization effect is featured by the increase/decrease of its conduction band bottom potential, in agreement with the experiments.[18,54] Thermodynamically, the transfer of excited electrons into the conduction band of the TiO_2 NB can only occur when the conduction band edge of the CdSe QDs is higher than that of the TiO_2 NB. The DOS in Figure 2 demonstrates that the QD sensitizes the semiconductor by introducing electronic states in the semiconductor band gap. Furthermore, Figure 2 shows that the QD introduces excited electronic states that overlap in energy with electronic states in the conduction band of the TiO_2 NB. The smaller QD particle size has a higher conduction band edge, and therefore, a higher driving force for injecting electrons into the conduction band of the TiO_2 NB. The LUMO of the combined CdSe-TiO_2 system is due to TiO_2, while the HOMO arises from the CdSe QD.

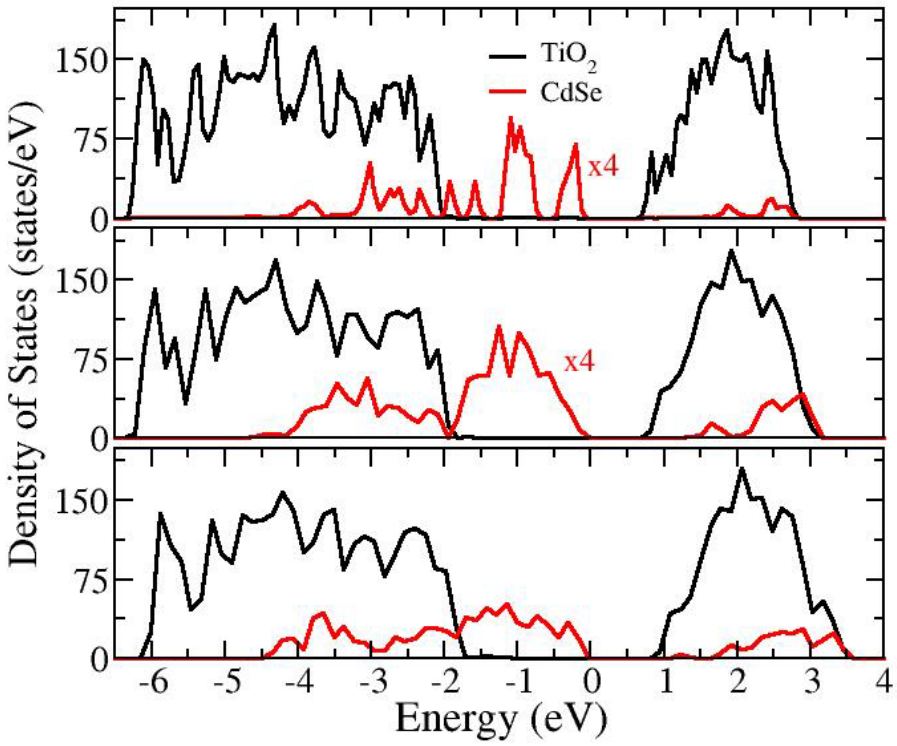

Figure 2. Density of states of the TiO_2 NB (black line) and CdSe QD (red line). The Fermi level is set to zero. Top: Cd_6Se_6-TiO_2 NB; middle: $Cd_{13}Se_{13}$-TiO_2 NB; bottom: $Cd_{36}Se_{36}$-TiO_2 NB. The Cd_6Se_6 and $Cd_{13}Se_{13}$ DOS have been rescaled by a factor of 4 for clarity.

Changes in the QD size affect both donor-acceptor coupling and energy. The strength of the donor-acceptor coupling is directly reflected in the amount of mixing between the donor and acceptor orbitals. Generally, the stronger is the electronic interaction, the more significant is the mixing. Figure 3 shows the spatial distribution of electron densities of the donor and acceptor states for the electron injection process. The QD LUMO is the donor state for the charge separation. In all three systems, the donor state is delocalized over the whole QD, Figure 3(a), (d) and (g).

It should be noted that the band states of an isolated TiO_2 NB are delocalized. However, the acceptor states seen in the QD-NB system are localized, because the adsorbed donor breaks the symmetry. The acceptor states are not uniformly spread over the NB and are localized towards the region where the binding interaction between CdSe and TiO_2 is strongest. This is a generic phenomenon found in other systems, for instance at a molecular chromophore-TiO_2 interface.[55] The weak donor-acceptor coupling in the CdSe-QD/TiO_2-NB system, and the large ensemble of available phonon modes, cause the excited electron to be transferred from the QD donor to the NB acceptor state by a NA transition, and the excess electronic energy to be deposited into vibrational modes.

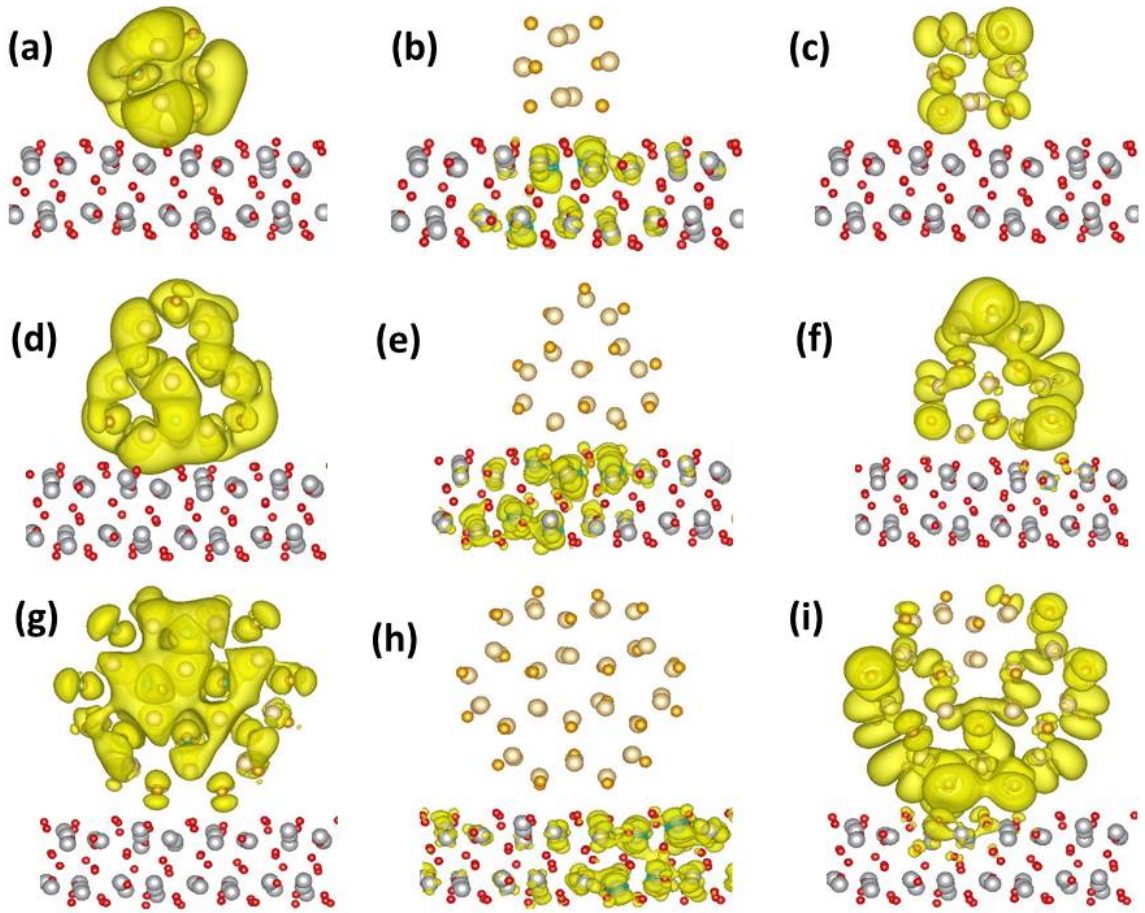

Figure 3. Charge densities of (1st column) QD donor states, (2nd column) TiO_2 acceptor states, and (3rd column) QD HOMO states of the Cd_nSe_n-TiO_2 systems. The 1st, 2nd, and 3rd rows are for n = 6, 13, and 36, respectively.

In our recent publication,[17] we tested the results with respect to the size of the nanobelt. We carried out additional calculations with $Cd_{13}Se_{13}$ adsorbed on a 50% thicker TiO_2 nanobelt and identified the acceptor state. Similarly to the example in the text, the acceptor state was not uniformly spread over the NB and was localized towards the region where the binding interaction between CdSe and TiO_2 was strongest. At the same time, the acceptor state became more delocalized in the thicker slab. One can expect that some degree of localization of the acceptor state should remain even in thick NBs, because the NB symmetry is broken by interaction with the CdSe QD.

3.2 Vibrational motions contributing to the ET dynamics

Vibrational motions alter the atomic coordinates of the CdSe QD and TiO_2 NB, generate a distribution of the photoexcited state energies, and create an inhomogeneous ensemble of initial conditions for the photoinduced ET processes.[9] Vibrations are also responsible for fluctuation of the energy gap between the donor and acceptor states. They generate the nonadiabatic coupling, that causes hops between adiabatic states. Finally, vibrations accommodate the excess electronic energy released during the ET process. The fluctuations of the QD HOMO and LUMO, and the NB LUMO due to thermal atomic motions are shown in Figure 4. The small energy fluctuations of the CdSe QD HOMO and LUMO are reasonable. The QD is composed of heavy atoms and exhibits high symmetry. Heavy atoms move little, and the QD symmetry is preserved. The fluctuations are much larger for the smallest QD studied and decrease with the increase of the particle size. QDs become more rigid with increasing size, and their geometries change much less due to thermal fluctuations and electronic excitation. The averaged gaps between the QD and NB LUMOs during the MD run are 1.14, 0.83 and 0.29 eV, for n = 6, 13 and 36, respectively. The relative magnitudes of the gaps and the trend agree well with the experimental data.[19,54]

To characterize the randomness of the phonon-induced fluctuation in the electronic excitation energy gap, we compute the autocorrelation functions (ACFs), commonly used for chemical kinetics studies[56-58] and defined as

$$C(t) = \frac{\langle E(t)E(0)\rangle}{\langle E^2\rangle} \tag{1}$$

where $E(t)$ is the energy gap between a given pair of states. The ACFs quantify the memory of the corresponding fluctuations. The ACFs for the transition between the QD LUMO and the NB LUMO are shown in Figure 5 (black lines). The ACFs show a significantly faster decay for Cd_6Se_6 and $Cd_{13}Se_{13}$

compared to $Cd_{36}Se_{36}$. The decay time scales are approximatively 11 fs for Cd_6Se_6 and $Cd_{13}Se_{13}$ and 124 fs for $Cd_{36}Se_{36}$. The rapid decay in Cd_6Se_6 and $Cd_{13}Se_{13}$ is a result of the coupling of the electronic subsystem to more phonon modes compared to $Cd_{36}Se_{36}$.

Taking the Fourier transform of the ACFs helps to identify the phonon modes that couple to the electronic subsystem and promote the ET. FTs were computed from 1 ps trajectories, allowing frequency resolution of ~75 cm^{-1}. Figure 6 shows the data for the charge separation process (black lines) in the three systems. For the system with the smallest QD, the dominant peak appears at 852 cm^{-1} and can be attributed to the longitudinal optical phonon mode of TiO_2. The dominant peak for the two other systems appears at around 100 cm^{-1}, in the range of acoustic modes that modulate the size and shape of the NB.

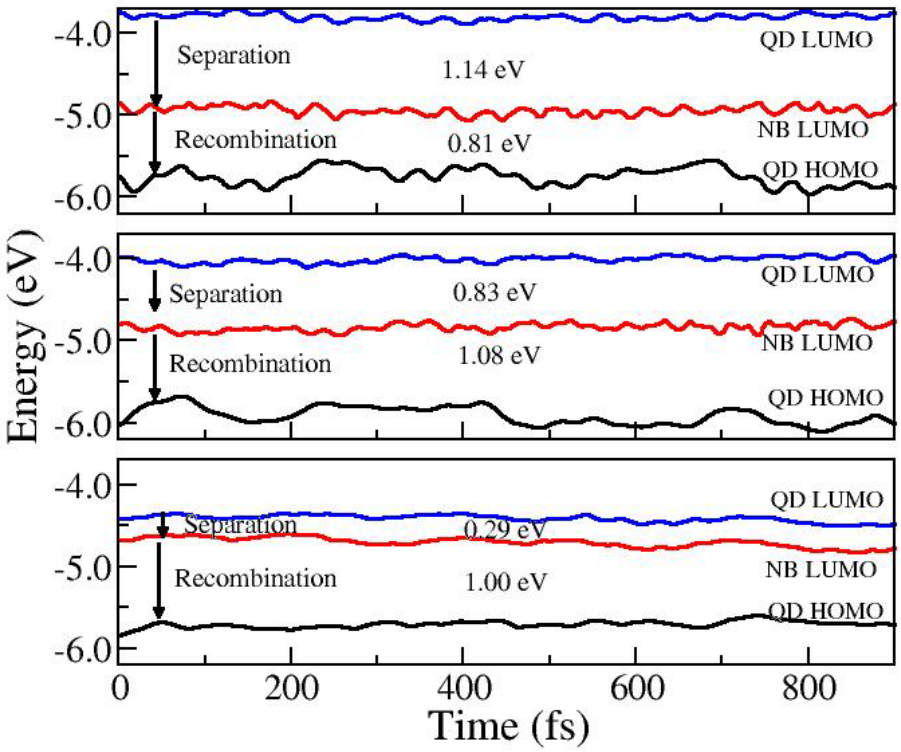

Figure 4. Evolution of the energies of the QD LUMO (blue line) and HOMO (black line), and the NB LUMO (red line). Top: Cd_6Se_6-TiO_2 NB; middle: $Cd_{13}Se_{13}$-TiO_2 NB; bottom: $Cd_{36}Se_{36}$-TiO_2 NB.

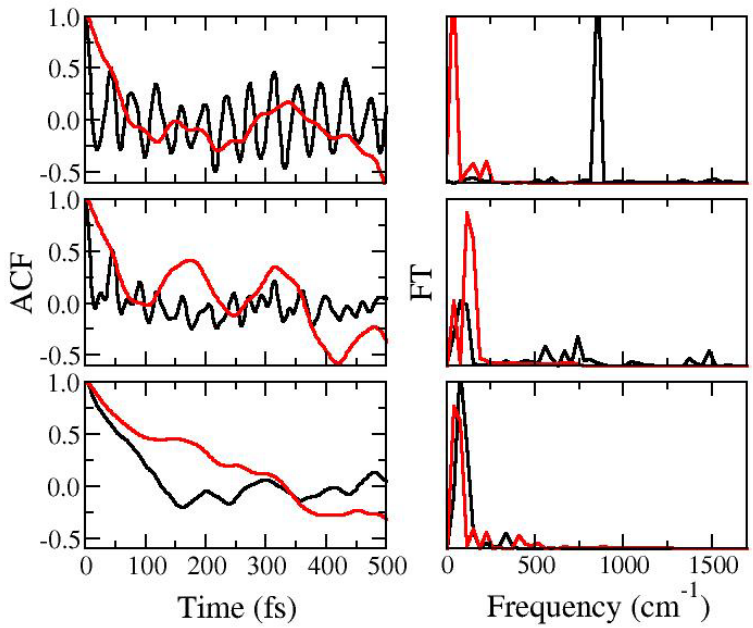

Figure 5. (Left) Autocorrelation functions and (right) Fourier transforms of the electronic energy gaps between the QD LUMO and the NB LUMO (black line), and between the NB LUMO and the QD HOMO (red line). Top: Cd_6Se_6-TiO_2 NB; middle: $Cd_{13}Se_{13}$-TiO_2 NB; bottom: $Cd_{36}Se_{36}$-TiO_2 NB.

3.3 Electron transfer dynamics

The ET from the CdSe to TiO_2 NB occurs via a NA transition between the corresponding states.[17] The time-dependent populations of the donor states for the charge separation illustrate the evolution of the ET process in Figure 6. The time scales for the ET are obtained by fitting the data by a combined exponential and Gaussian function

$$f(t) = Bexp\left(-\frac{t}{\tau_1}\right) + (1-B)exp\left(-0.5\left(\frac{t}{\tau_2}\right)^2\right) \tag{2}$$

f(t) is the fitting function of the time-dependent populations of the donor states shown in Figures 6 and 7. Generally, quantum dynamics starts with a cosine/Gaussian time-dependence, as in the Rabi oscillation. As the number of quantum states involved in the dynamics grows, the time-dependence becomes

exponential, as in Fermi's golden rule. These two regimes, seen in Figures 6 and 7, are represented by the fitting function, eq 2. The ET times,τ, reported in the figures are computed as weighted averages of the exponential and Gaussian components: $\tau = B\tau_1 + (1 - B)\tau_2$. The photoinduced ET from the Cd_6Se_6, $Cd_{13}Se_{13}$, and $Cd_{36}Se_{36}$ QDs into the TiO_2 NB occur on different time scales, 20 fs, 21 fs and 158 fs, respectively. These results correspond to the faster end of the broad range of the experimental injection times measured for a variety of CdSe-TiO_2 systems.[19,54,59] In particular, the simulated times are in agreement with the 1.68×10^{11} s^{-1} transfer rate measured by Tvrdy *et al*. for their smallest CdSe nanoparticle (2.8 nm diameter).[54] It should be noted that the systems used in the calculations are smaller than those in the experiment. For example, our largest QD size is 1.30 nm which is less than half the 2.8 nm diameter reported by Tvrdy *et al*. Because of the reduced system size, one expects the simulated dynamics to be faster than the measured time scales in general. Besides the system size, various other parameters can influence ET times obtained in experiment, including preparation methods, surface roughness of QD and substrate, and linker.

According to the Marcus theory, the logarithm of the ET rate for a non-adiabatic reaction in the classical limit is a quadratic function with respect to the driving force.[60,61] As the driving force increases, the ET rate increases as well, and reaches a maximum when the driving force equals the reorganization energy. The TiO_2 density of states at the QD LUMO energy depends on the offset between the QD LUMO and the bottom edge of the TiO_2 conduction band, as shown, for instance, in the experiments by Robel *et al*.[19] Data in Figure 6 shows that as the QD size increases, the ET rate is enhanced. In other words, the ET time increases as the band gap decreases. Hence, the ET rate is intimately related to the energy gap, in good agreement with the experiments.[19,54] The fastest ET in our simulated CdSe-TiO_2 systems is observed with Cd_6Se_6 QD, which indicates that smaller-sized CdSe quantum dots show greater charge injection rates, *a priori* desirable for high efficiency devices. However, larger particles have better absorption in the visible region but cannot inject electrons into TiO_2 as effectively as smaller-sized CdSe

quantum dots. Often, faster charge separation correlates with faster charge recombination, which is detrimental for device performance.

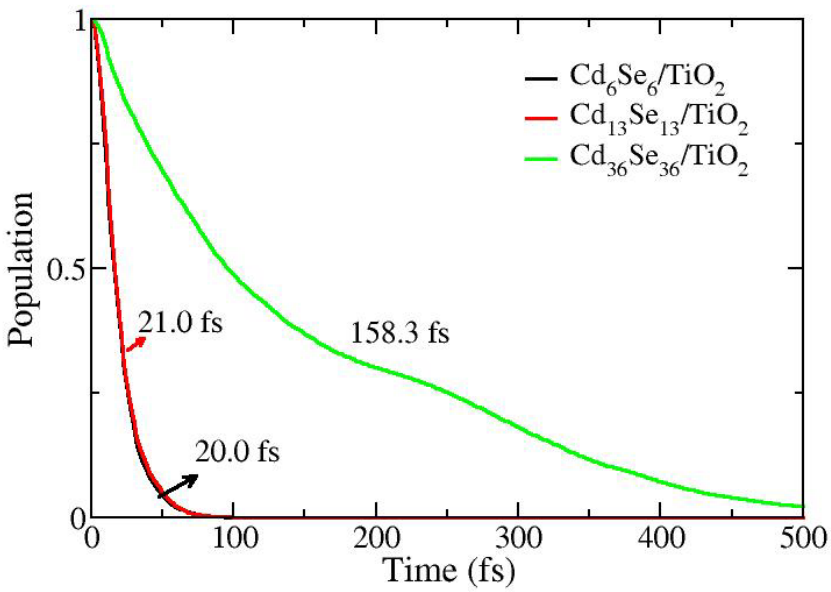

Figure 6. Electron transfer from the CdSe QD LUMO to the TiO_2 NB LUMO, represented by the time-dependent populations of the donor orbital. The time constants are obtained by a combined exponential and Gaussian fits, eq 2.

3.4 Electron-Hole Recombination

The return of the electron from the TiO_2 NB to the CdSe QD occurs by a transition from the bottom of the TiO_2 conduction band to the QD HOMO. Decreasing the QD gap lowers the LUMO energy and increases the donor-acceptor gap. Due to this large energy gap that separates the donor and acceptor states for charge recombination, and the excess electronic energy that is accommodated by phonons, it is very unlikely that a nuclear fluctuation can bring the initial (donor) and final (acceptor) electronic states in resonance. Therefore, it will necessitate a nonadiabatic transition to transfer the electrons back to the CdSe QD. Figure 3 (2nd and 3rd columns) depicts the charge densities of TiO_2 LUMOs and QD HOMOs,

which constitute the initial and final states for the electron-hole recombination. The LUMOs are localized in the TiO_2, because the adsorbed donor breaks the symmetry. The HOMOs are localized on Cd_nSe_n (n = 6, 13, 36) and extend into the TiO_2 substrate for n = 13 and 36.

The evolution of the energy gaps between the NB LUMO and the QD HOMO as a function of time is plotted in Figure 4. As the size of the QD increases, the average energy gap increases and the fluctuations decrease. Figure 5 presents the ACFs of the HOMO-LUMO energy gap for all the systems studied. The ACFs are different to those for the electron injection. Their oscillation periods are longer, and their decay time scales are 71, 92 and 332 fs for Cd_6Se_6, $Cd_{13}Se_{13}$, and $Cd_{36}Se_{36}$, respectively. The Fourier transform of these energy gaps are also presented in Figure 5. Their spectra show a stronger contribution from the low frequency vibrations at around 37 cm^{-1}, and in the 111-250 cm^{-1} energy window.

The time-dependent populations of the donor states for the recombination process are illustrated in Figure 7. The calculated times obtained using the combined exponential and Gaussian function, eq 2, are 0.45, 0.69, and 1.70 ps for Cd_6Se_6, $Cd_{13}Se_{13}$, and $Cd_{36}Se_{36}$, respectively. The electron-hole recombination trend is similar to that for the charge separation, with slower recombination time for larger QDs. The effect of increasing QD size on the recombination rate is significant, consistent with the experimental observation.[62] Our simulations show that larger QDs suppress the electron-hole recombination.

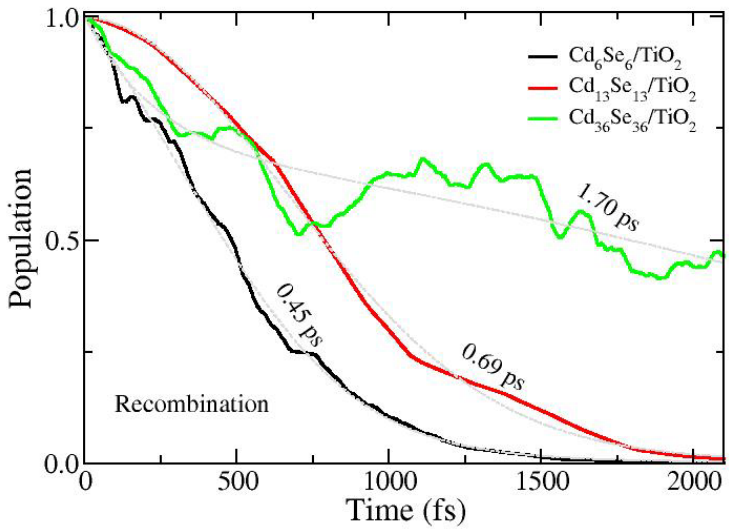

Figure 7. Electron transfer from the TiO_2 LUMO to the CdSe HOMO, resulting in electron-hole recombination and represented by the time-dependent populations of the initial state.

3.5 Temperatures Effects on the Interfacial ET Dynamics

Probing the temperature dependence of ET reactions can give additional information regarding their mechanism. Only a few studies of the temperature dependence of fast ET reactions using femtosecond transient absorption spectroscopy have been reported to date.[21,63,64] The problem is due to the experimental difficulties associated with performing temperature-dependent pump-probe experiments. We have performed a series of simulations on the Cd_6Se_6/TiO_2 and $Cd_{36}Se_{36}/TiO_2$ system at temperatures ranging from 100 to 300 K to study the temperature dependence of the charge separation and charge recombination processes at the CdSe-TiO_2 interface. By fitting the charge separation ET rate for each temperature to the combined exponential and Gaussian function, eq 2, we can plot the logarithm of the ET rate ($k_{ET} = 1/\tau$) as a function of inverse temperature, Figure 8. Overall, the data follows Arrhenius behavior, indicating that photoinduced electron injection can be modeled using the expression

$$k_{ET} = \kappa_{el}\nu \exp(-\frac{\Delta G}{k_B T}) \tag{3}$$

where ΔG is the Gibbs free energy of activation, κ_{el} is the electronic transmission coefficient which is usually estimated to be unity according to the classical Marcus theory, v is the frequency of nuclear motion over the barrier, T is the temperature, and k_B is the Boltzmann constant. A linear regression of the data gives ΔG = 0.006 eV, which corresponds to k_BT at 66 K for Cd_6Se_6/TiO_2; and ΔG = 0.014 eV, which corresponds to k_BT at 163 K for $Cd_{36}Se_{36}/TiO_2$. The frequency prefactors determined by the Arrhenius fit are equal to 9.30×10^{13} and 2.44×10^{13} s^{-1} for Cd_6Se_6/TiO_2 and $Cd_{36}Se_{36}/TiO_2$, respectively. The calculated energy of activation depends on the size of the QD and it increases with the QD's size.

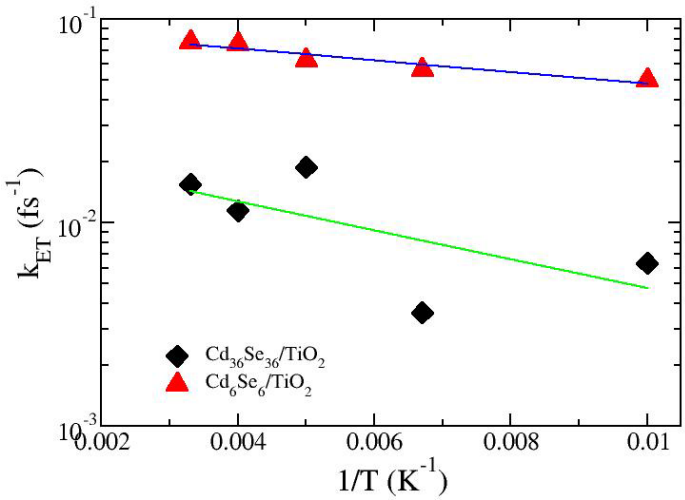

Figure 8. Electron transfer rate in the $Cd_{36}Se_{36}$-TiO_2 system as a function of temperature. The ET rate shows an Arrhenius dependence on temperature, as in the Marcus theory.

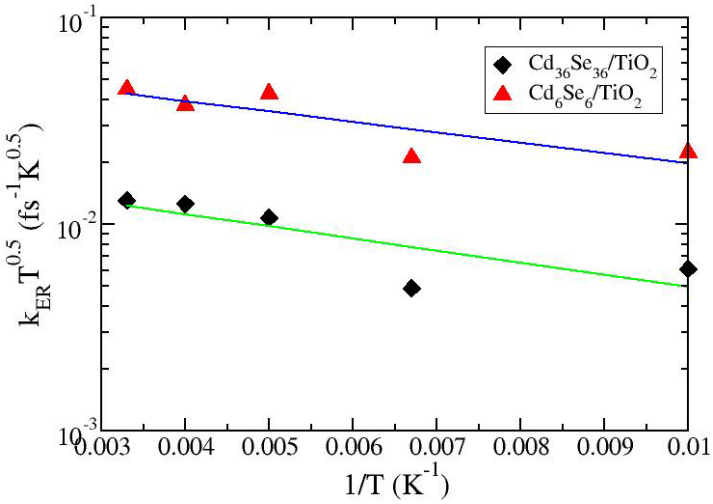

Figure 9. Charge recombination rate (k_{ER}=1/τ) times $T^{1/2}$ as a function of temperature for Cd_6Se_6/TiO_2 (triangle) and $Cd_{36}Se_{36}/TiO_2$ (diamond). The lines are fit to the linearized form of eq 4.

The temperature dependence of the charge recombination rate constant is expected to follow the Marcus equation (eq 4):

$$k_{ER} = \sqrt{\frac{\pi}{\hbar^2 \lambda k_B T}} |V|^2 exp\left[-\frac{(\Delta G^0 + \lambda)^2}{4\lambda k_B T}\right] \tag{4}$$

where V is the electronic coupling, λ the reorganization energy accompanying the redistribution of charge, and ΔG^0 the thermodynamic driving force for the ET process. Rewriting this equation shows that a plot of $\ln\left(k_{ER}T^{1/2}\right)$ versus $1/T$ is linear. Therefore, the electronic coupling V can be obtained from the intercept of the plot, and the slope gives the reorganization energy λ or the thermodynamic driving force ΔG^0 providing that one of the two quantities is known. The reorganization energy that accounts for energy fluctuations in the system due to charge transfer has been reported to have characteristic small values of tens of millielectronvolts for nanocrystals.[54,65] In Figure 9, the rate constants for the charge recombination in Cd_6Se_6/TiO_2 and $Cd_{36}Se_{36}/TiO_2$ are plotted against inverse temperature and fitted to the linearized form of eq 4. Our results show that the recombination rates slowly increase with temperature. Since our

calculations are done in vacuum and because of a weak exciton-phonon coupling, the reorganization energy is expected to be very small with only vibrational modes contributing.[65] Taking λ = 10.0 meV, as reported by Tvrdy *et al*.,[54] the optimized values of ΔG^0 and V were estimated and reported in Table 1. For both systems, the electronic coupling is of the same order of magnitude, 37.4 cm^{-1} for Cd_6Se_6/TiO_2 and 20.8 cm^{-1} for $Cd_{36}Se_{36}/TiO_2$. By using the same reorganization energy value for both systems, we observe that the effect of the QD size on the driving force is very small. These results suggest that the decrease in the recombination rate for larger dots arises mainly from the donor-acceptor coupling rather than the changes in the energy gap. This is confirmed by the analytic analysis presented in.[66]

Both charge separation and recombination rates depend strongly on the QD size, with higher rates for smaller QDs, see Figure 8 and 9. The dynamics is slower in larger dots, because QD states are more delocalized and donor-acceptor couplings are smaller. The size dependence is slightly stronger for the injection and recombination. The electron requires more time to move around larger QDs to find the interface and transfer to TiO_2. The recombination can involves QD states that are localized towards TiO_2, e.g. Figure 3i, and therefore it is less sensitive to the overall QD size than injection. As the QD keeps increasing to the bulk limit, the electron injection rate should continue to grow, while the recombination rate can be expected to reach a limiting value.

Table 1. Driving forces ($\boldsymbol{\Delta G^0}$), reorganization energies (λ), and electronic couplings (V) for charge recombination in CdSe-TiO_2 obtained from fitting the calculated rate constants ($\boldsymbol{k_{ER}}$) to eq 4.

System	λ (meV)	V (cm^{-1})	ΔG^0 (eV)
Cd_6Se_6/TiO_2	10.0	37.4	-0.030
$Cd_{36}Se_{36}/TiO_2$	10.0	20.8	-0.032

The Marcus theory analysis is performed only for the electron-hole recombination reaction, because it can be described by a simple reactant-product scheme involving one donor and one acceptor state, occupied by electron and hole. The forward ET requires more advanced analytic treatments,[67 68] since it involves a high density of TiO_2 acceptor states which are close in energy to the QD LUMO.

The data in Table 1 implies that the electron-hole recombination reaction occurs in the Marcus inverted region, which may involve quantum-mechanical tunneling in the nuclear degrees of freedom. Nuclear tunneling is not included in the present NAMD simulations. Semiclassical treatments of nuclei make NAMD simulations significantly more expensive and impossible to perform on current systems. The current work focuses on the ab initio time-domain simulation, and the Marcus type rate description is used here to analyze the simulation data. Both atomistic simulation and analytic theory exclude nuclear tunneling. One can expect that the nuclear tunneling effect is small in the present systems, because they are composed of only heavy elements: Cd, Se, Ti and O.

4. CONCLUSIONS

We have performed NAMD simulations combined with time-domain DFT to characterize in detail transfer of the photogenerated electron from a series of CdSe QDs (sizes 0.5, 1.0, and 1.3 nm in diameter) to a TiO_2 NB and from a TiO_2 NB back to the CdSe QDs. The simulated time scales for both ET and charge recombination agree with the experimental observations. The simulations indicate that both charge separation and recombination rates strongly depend on the QD size, with higher rates for smaller QDs. The dynamics is slower in larger dots, because QD states are more delocalized and donor-acceptor couplings are smaller. The size dependence is slightly stronger for the injection and recombination. The adsorption of CdSe breaks the symmetry of delocalized band-type states of the TiO_2 NB, creating localized states. The donor states of the photoinduced charge separation and the acceptor states of the photoinduced charge recombination are strongly localized on the QDs. The ET rate exhibits

an Arrhenius-type temperature dependence, with activation of the order of millielectronvolts. Simulations suggest that temperature dependence of the charge recombination rate can be successfully modeled using the Marcus equation through optimization of the electronic coupling and reorganization energy. Reasonable values for the electronic couplings and driving forces were extracted from fits of the temperature variation of the recombination rates. The study provides valuable insights into the dynamics of the interfacial charge separation and recombination, important to a wide variety of applications, including solar cells, light emitting diodes, and photocatalysis.

Corresponding Authors

*Email: denyago.tafen@contr.netl.doe.gov. Phone: +1 (541) 918-4462

*Email: prezhdo@usc.edu. Phone:

ACKNOWLEDGMENTS

The technical effort was performed in support of the National Energy Technology Laboratory's ongoing research under the RES Contract DE-FE0004000. Part of this research used resources of the National Energy Research Scientific Computing Center, which is supported by the Office of Science of the U.S. Department of Energy under Contract No. DE-AC02-05CH11231. DNT would like to thank C. Matranga for fruitful discussions. OVP acknowledges financial support of the US Department of Energy, grant # DE-SC0006527. This project was funded by the Department of Energy, National Energy Technology Laboratory, an agency of the United States Government, through a support contract with URS Energy &Construction, Inc. Neither the United States Government nor any agency thereof, nor any of their employees, nor URS Energy & Construction, Inc., nor any of their employees, makes any warranty, expressed or implied, or assumes any legal liability or responsibility for the accuracy, completeness, or usefulness of any information, apparatus, product, or process disclosed, or represents that its use would not infringe privately owned rights. Reference herein to any specific commercial

product, process, or service by trade name, trademark, manufacturer, or otherwise, does not necessarily constitute or imply its endorsement, recommendation, or favoring by the United States Government or any agency thereof. The views and opinions of authors expressed herein do not necessarily state or reflect those of the United States Government or any agency thereof.

REFERENCES

(1) Fujishima, A.; Honda, K. Electrochemical Photolysis of Water at a Semiconductor Electrode. *Nature* **1972**, *238*, 37-38.

(2) Diebold, U. Photocatalysts: Closing the Gap. *Nat. Chem.* **2011**, *3*, 271-272.

(3) Murdoch M; Waterhouse, G. I. N.; Nadeem, M. A.; Metson, J. B.; Keane, M. A.; Howe, R. F.; Llorca J.; Idriss H. The Effect of Gold Loading and Particle Size on Photocatalytic Hydrogen Production from Ethanol over Au/TiO_2 Nanoparticles. *Nat. Chem.* **2011**, *3*, 489-492.

(4) O'Regan, B.; Gratzel, M. A Low-Cost, High-Efficiency Solar Cell Based on Dye-Sensitized Colloidal TiO_2 Films. *Nature* **1991**, *353*, 737-740.

(5) Nishimura, S.; Abrams, N.; Lewis, B. A.; Halaoui, L. I.; Mallouk, T. E.; Benkstein, K. D.; van de Lagemaat, J.; Frank, A. J. Standing Wave Enhancement of Red Absorbance and Photocurrent in Dye-Sensitized Titanium Dioxide Photoelectrodes Coupled to Photonic Crystals. *J. Am. Chem. Soc.* **2003**, *125*, 6306-6310.

(6) Asahi, R.; Morikawa, T.; Ohwaki, T.; Aoki, K.; Taga, Y. Visible-Light Photocatalysis in Nitrogen-Doped Titanium Oxides. *Science* **2001**, *293*, 269-271.

(7) Wang, J.; Tafen, D. N.; Lewis, J. P.; Hong, Z.; Manivannan, A.; Zhi, M.; Li, M.; Wu, N. Origin of Photocatalytic Activity of Nitrogen-Doped TiO_2 Nanobelts. *J. Am. Chem. Soc.* **2009**, *131*, 12290-12297.

(8) Duncan, W. R.; Prezhdo, O. V. Theoretical Studies of Photoinduced Electron Transfer in Dye-Sensitized TiO_2. *Annu. Rev. Phys. Chem.* **2007**, *58*, 143-184.

(9) Duncan, W. R.; Prezhdo, O. V. Temperature Independence of the Photoinduced Electron Injection in Dye-Sensitized TiO_2 Rationalized by Ab Initio Time-Domain Density Functional Theory. *J. Am. Chem. Soc.* **2008**, *130*, 9756-9762.

(10) Kitamura, T.; Ikeda, M.; Shigaki, K.; Inoue, T.; Anderson, N. A.; Ai, X.; Lian, T.; Yanagida, S. Phenyl-Conjugated Oligoene Sensitizers for TiO_2 Solar Cells. *Chem. Mater.* **2004**, *16*, 1806-1812.

(11) da Silva, R.; Rego, L. G. C.; Freire, J. A.; Rodriguez, J.; Laria, D.; Batista, V. S. Study of Redox Species and Oxygen Vacancy Defects at TiO2-Electrolyte Interfaces. *J. Phys. Chem. C* **2010**, *114*, 19433-19442.

(12) van Hal, P. A.; Christiaans, M. P. T.; Wienk, M. M.; Kroon, J. M.; Janssen, R. A. J. Photoinduced Electron Transfer from Conjugated Polymers to TiO_2. *J. Phys. Chem. B* **1999**, *103*, 4352-4359.

(13) Lin, Y.-Y.; Chu, T.-H.; Li, S.-S.; Chuang, C.-H.; Chang, C.-H.; Su, W.-F.; Chang, C.-P.; Chu, M.-W.; Chen, C.-W. Interfacial Nanostructuring on the Performance of Polymer/TiO_2 Nanorod Bulk Heterojunction Solar Cells. *J. Am. Chem. Soc.* **2009**, *131*, 3644-3649.

(14) Fang, Z.; Eshbaugh, A. A.; Schanze, K. S. Low-Bandgap Donor−Acceptor Conjugated Polymer Sensitizers for Dye-Sensitized Solar Cells. *J. Am. Chem. Soc.* **2011**, *133*, 3063-3069.

(15) Long, R.; English, N. J.; Prezhdo, O. V. Photo-Induced Charge Separation across the Graphene–TiO_2 Interface Is Faster than Energy Losses: A Time-Domain ab Initio Analysis. *J. Am. Chem. Soc.* **2012**, *134*, 14238-14248.

(16) Long, R.; Dai, Y.; Huang, B. Fullerene Interfaced with a TiO_2(110) Surface May Not Form an Efficient Photovoltaic Heterojunction: First-Principles Investigation of Electronic Structures. *J. Phys. Chem. Lett.* **2013**, *4*, 2223-2229.

(17) Tafen, D. N.; Long, R.; Prezhdo, O. V. Dimensionality of Nanoscale TiO_2 Determines the Mechanism of Photoinduced Electron Injection from a CdSe Nanoparticle. *Nano Lett.* **2014**, *14*, 1790-1796.

(18) Kongkanand, A.; Tvrdy, K.; Takechi, K.; Kuno, M.; Kamat, P. V. Quantum Dot Solar Cells. Tuning Photoresponse through Size and Shape Control of CdSe−TiO_2 Architecture. *J. Am. Chem. Soc.* **2008**, *130*, 4007-4015.

(19) Robel, I.; Kuno, M.; Kamat, P. V. Size-Dependent Electron Injection from Excited CdSe Quantum Dots into TiO_2 Nanoparticles. *J. Am. Chem. Soc.* **2007**, *129*, 4136-4137.

(20) Robel, I.; Subramanian, V.; Kuno, M.; Kamat, P. V. Quantum Dot Solar Cells. Harvesting Light Energy with CdSe Nanocrystals Molecularly Linked to Mesoscopic TiO_2 Films. *J. Am. Chem. Soc.* **2006**, *128*, 2385-2393.

(21) Tisdale, W. A.; Williams, K. J.; Timp, B. A.; Norris, D. J.; Aydil, E. S.; Zhu, X. Y. Hot-Electron Transfer from Semiconductor Nanocrystals. *Science* **2010**, *328*, 1543-1547.

(22) Liu, Z.; Zhu, H.; Song, N.; Lian, T. Probing Spatially Dependent Photoinduced Charge Transfer Dynamics to TiO_2 Nanoparticles Using Single Quantum Dot Modified Atomic Force Microscopy Tips. *Nano Lett.* **2013**, *13*, 5563-5569.

(23) Yang, Y.; Rodríguez-Córdoba, W.; Xiang, X.; Lian, T. Strong Electronic Coupling and Ultrafast Electron Transfer between PbS Quantum Dots and TiO_2 Nanocrystalline Films. *Nano Lett.* **2011**, *12*, 303-309.

(24) Hyun, B.-R.; Bartnik, A. C.; Sun, L.; Hanrath, T.; Wise, F. W. Control of Electron Transfer from Lead-Salt Nanocrystals to TiO_2. *Nano Lett.* **2011**, *11*, 2126-2132.

(25) Wang, C.; Thompson, R. L.; Ohodnicki, P.; Baltrus, J.; Matranga, C. Size-Dependent Photocatalytic Reduction of CO_2 with PbS Quantum Dot Sensitized TiO_2 Heterostructured Photocatalysts. *J. Mater. Chem.* **2011**, *21*, 13452-13457.

(26) Wang, C.; Thompson, R. L.; Baltrus, J.; Matranga, C. Visible Light Photoreduction of CO_2 Using CdSe/Pt/TiO_2 Heterostructured Catalysts. *J. Phys. Chem. Lett.* **2009**, *1*, 48-53.

(27) Nozik, A. J.; Beard, M. C.; Luther, J. M.; Law, M.; Ellingson, R. J.; Johnson, J. C. Semiconductor Quantum Dots and Quantum Dot Arrays and Applications of Multiple Exciton Generation to Third-Generation Photovoltaic Solar Cells. *Chem. Rev.* **2010**, *110*, 6873-6890.

(28) McGuire, J. A.; Joo, J.; Pietryga, J. M.; Schaller, R. D.; Klimov, V. I. New Aspects of Carrier Multiplication in Semiconductor Nanocrystals. *Acc. Chem. Res.* **2008**, *41*, 1810-1819.

(29) Wang, D.; Zhao, H.; Wu, N.; El Khakani, M. A.; Ma, D. Tuning the Charge-Transfer Property of PbS-Quantum Dot/TiO_2-Nanobelt Nanohybrids via Quantum Confinement. *J. Phys. Chem. Lett.* **2010**, *1*, 1030-1035.

(30) Allam, N. K.; Poncheri, A. J.; El-Sayed, M. A. Vertically Oriented Ti–Pd Mixed Oxynitride Nanotube Arrays for Enhanced Photoelectrochemical Water Splitting. *ACS Nano* **2011**, *5*, 5056-5066.

(31) Wei, W.; Bao, X.-Y.; Soci, C.; Ding, Y.; Wang, Z.-L.; Wang, D. Direct Heteroepitaxy of Vertical InAs Nanowires on Si Substrates for Broad Band Photovoltaics and Photodetection. *Nano Lett.* **2009**, *9*, 2926-2934.

(32) Craig, C. F.; Duncan, W. R.; Prezhdo, O. V. Trajectory Surface Hopping in the Time-Dependent Kohn-Sham Approach for Electron-Nuclear Dynamics. *Phys. Rev. Lett.* **2005**, *95*, 163001-163004.

(33) Fischer, S. A.; Habenicht, B. F.; Madrid, A. B.; Duncan, W. R.; Prezhdo, O. V. Regarding the Validity of the Time-Dependent Kohn-Sham Approach for Electron-Nuclear Dynamics via Trajectory Surface Hopping. *J. Chem. Phys.* **2011**, *134*, 024102-9.

(34) Tully, J. C. Molecular Dynamics with Electronic Transitions. *J. Chem. Phys.* **1990**, *93*, 1061-1071.

(35) Parandekar, P. V.; Tully, J. C. Mixed Quantum-Classical Equilibrium. *J. Chem. Phys.* **2005**, *122*, 094102.

(36) Habenicht, B. F.; Prezhdo, O. V. Nonradiative Quenching of Fluorescence in a Semiconducting Carbon Nanotube: A Time-Domain Ab Initio Study. *Phys. Rev. Lett.* **2008**, *100*, 197402.

(37) Habenicht, B. F.; Prezhdo, O. V. Time-Domain Ab Initio Study of Nonradiative Decay in a Narrow Graphene Ribbon. *J. Phys. Chem. C* **2009**, *113*, 14067-14070.

(38) Chaban, V. V.; Prezhdo, V. V.; Prezhdo, O. V. Covalent Linking Greatly Enhances Photoinduced Electron Transfer in Fullerene-Quantum Dot Nanocomposites: Time-Domain Ab Initio Study. *J. Phys. Chem. Lett.* **2012**, *4*, 1-6.

(39) Long, R.; Prezhdo, O. V. Ab Initio Nonadiabatic Molecular Dynamics of the Ultrafast Electron Injection from a PbSe Quantum Dot into the TiO_2 Surface. *J. Am. Chem. Soc.* **2011**, *133*, 19240-19249.

(40) Long, R.; English, N. J.; Prezhdo, O. V. Defects Are Needed for Fast Photo-Induced Electron Transfer from a Nanocrystal to a Molecule: Time-Domain Ab Initio Analysis. *J. Am. Chem. Soc.* **2013**, *135*, 18892-18900.

(41) Long, R.; Prezhdo, O. V. Instantaneous Generation of Charge-Separated State on TiO_2 Surface Sensitized with Plasmonic Nanoparticles. *J. Am. Chem. Soc.* **2014**, *136*, 4343-4354.

(42) Hyeon-Deuk, K.; Prezhdo, O. V. Time-Domain ab Initio Study of Auger and Phonon-Assisted Auger Processes in a Semiconductor Quantum Dot. *Nano Lett.* **2011**, *11*, 1845-1850.

(43) Kilina, S. V.; Kilin, D. S.; Prezhdo, O. V. Breaking the Phonon Bottleneck in PbSe and CdSe Quantum Dots: Time-Domain Density Functional Theory of Charge Carrier Relaxation. *ACS Nano* **2008**, *3*, 93-99.

(44) Duncan, W. R.; Craig, C. F.; Prezhdo, O. V. Time-Domain ab Initio Study of Charge Relaxation and Recombination in Dye-Sensitized TiO_2. *J. Am. Chem. Soc.* **2007**, *129*, 8528-8543.

(45) Akimov, A. V.; Prezhdo, O. V. The PYXAID Program for Non-Adiabatic Molecular Dynamics in Condensed Matter Systems. *J. Chem. Theory Comput.* **2013**, *9*, 4959-4972.

(46) Akimov, A. V.; Prezhdo, O. V. Advanced Capabilities of the PYXAID Program: Integration Schemes, Decoherenc:e Effects, Multiexcitonic States, and Field-Matter Interaction. *J. Chem. Theory Comput.* **2014**, *10*, 789-804.

(47) Kresse, G.; Furthmüller, J. Efficient Iterative Schemes for Ab Initio Total-Energy Calculations Using a Plane-Wave Basis Set. *Phys. Rev. B* **1996**, *54*, 11169-11186.

(48) Perdew, J. P.; Burke, K.; Ernzerhof, M. Generalized Gradient Approximation Made Simple. *Phys. Rev. Lett.* **1996**, *77*, 3865-3868.

(49) Gundlach, L.; Ernstorfer, R.; Willig, F. Pathway-Dependent Electron Transfer for Rod-Shaped Perylene-Derived Molecules Adsorbed in Nanometer-Size TiO_2 Cavities. *J. Phys. Chem. C* **2007**, *111*, 13586-13594.

(50) Gundlach, L.; Ernstorfer, R.; Willig, F. Ultrafast Interfacial Electron Transfer from the Excited State of Anchored Molecules into a Semiconductor. *Prog. Surf. Sci.* **2007**, *82*, 355-377.

(51) Leforestier, C.; Bisseling, R. H.; Cerjan, C.; Feit, M. D.; Friesner, R.; Guldberg, A.; Hammerich, A.; Jolicard, G.; Karrlein, W.; Meyer, H. D.; et al. A Comparison of Different Propagation Schemes for the Time Dependent Schrödinger Equation. *J. Comput. Phys.* **1991**, *94*, 59-80.

(52) Rego, L. G. C.; Batista, V. S. Quantum Dynamics Simulations of Interfacial Electron Transfer in Sensitized TiO_2 Semiconductors. *J. Am. Chem. Soc.* **2003**, *125*, 7989-7997.

(53) Algar, W. R.; Wegner, D.; Huston, A. L.; Blanco-Canosa, J. B.; Stewart, M. H.; Armstrong, A.; Dawson, P. E.; Hildebrandt, N.; Medintz, I. L. Quantum Dots as Simultaneous Acceptors and Donors in Time-Gated Förster Resonance Energy Transfer Relays: Characterization and Biosensing. *J. Am. Chem. Soc.* **2012**, *134*, 1876-1891.

(54) Tvrdy, K.; Frantsuzov, P. A.; Kamat, P. V. Photoinduced Electron Transfer from Semiconductor Quantum Dots to Metal Oxide Nanoparticles. *Proc. Natl. Acad. Sci. U.S.A.* **2011**, *108*, 29-34.

(55) Duncan, W. R.; Stier, W. M.; Prezhdo, O. V. Ab Initio Nonadiabatic Molecular Dynamics of the Ultrafast Electron Injection across the Alizarin−TiO_2 Interface. *J. Am. Chem. Soc.* **2005**, *127*, 7941-7951.

(56) Neria, E.; Nitzan, A. Semiclassical Evaluation of Nonadiabatic Rates in Condensed Phases. *J. Chem. Phys.* **1993**, *99*, 1109-1123.

(57) Miller, W. H. Quantum-Mechanical Theory of Collisional Recombination Rates. *J. Phys. Chem.* **1995**, *99*, 12387-12390.

(58) Warshel, A.; Sussman, F.; Hwang, J. K. Evaluation of Catalytic Free-Energies in Genetically Modified Proteins. *J. Mol. Biol.* **1988**, *201*, 139-159.

(59) Pernik, D. R.; Tvrdy, K.; Radich, J. G.; Kamat, P. V. Tracking the Adsorption and Electron Injection Rates of CdSe Quantum Dots on TiO_2: Linked versus Direct Attachment. *J. Phys. Chem. C* **2011**, *115*, 13511-13519.

(60) Marcus, R. A. On the Theory of Electron-Transfer Reactions. VI. Unified Treatment for Homogeneous and Electrode Reactions. *J. Chem. Phys.* **1965**, *43*, 679-701.

(61) Marcus, R. A.; Sutin, N. Electron Transfers in Chemistry and Biology. *Biochim. Biophys. Acta - Reviews on Bioenergetics* **1985**, *811*, 265-322.

(62) Tisdale, W.; Zhu, X.-Y. Artificial Atoms on Semiconductor Surfaces. *Proc. Natl. Acad. Sci. U.S.A.* **2011**, *108*, 965-970.

(63) Kahnt, A.; Kärnbratt, J.; Esdaile, L. J.; Hutin, M.; Sawada, K.; Anderson, H. L.; Albinsson, B. Temperature Dependence of Charge Separation and Recombination in Porphyrin Oligomer–Fullerene Donor–Acceptor Systems. *J. Am. Chem. Soc.* **2011**, *133*, 9863-9871.

(64) Kuciauskas, D.; Liddell, P. A.; Lin, S.; Stone, S. G.; Moore, A. L.; Moore, T. A.; Gust, D. Photoinduced Electron Transfer in Carotenoporphyrin−Fullerene Triads: Temperature and Solvent Effects. *J. Phys. Chem. B* **2000**, *104*, 4307-4321.

(65) Scholes, G. D.; Jones, M.; Kumar, S. Energetics of Photoinduced Electron-Transfer Reactions Decided by Quantum Confinement. *J. Phys. Chem. C* **2007**, *111*, 13777-13785.

(66) Long, R.; English, N. J.; Prezhdo, O. V. Minimizing Electron-Hole Recombination on TiO_2 Sensitized with PbSe Quantum Dots: Time-Domain Ab Initio Analysis. *J. Phys. Chem. Lett.* **2014**, *5*, 2941-2946.

(67) Zhu, H.; Yang, Y.; Hyeon-Deuk, K.; Califano, M.; Song, N.; Wang, Y.; Zhang, W.; Prezhdo, O. V.; Lian, T. Auger-Assisted Electron Transfer from Photoexcited Semiconductor Quantum Dots. *Nano Lett.* **2014**, *14*, 1263-1269.

(68) Anderson, N. A.; Lian, T. Q. Ultrafast Electron Transfer at the Molecule-Semiconductor Nanoparticle Interface. *Annu. Rev. Phys. Chem.* **2005**, *56*, 491-519.
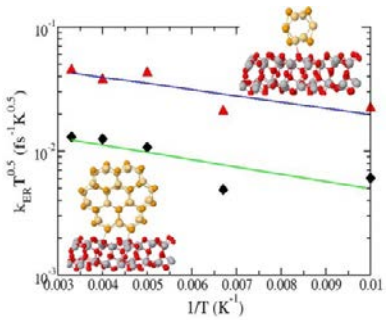
Table of Content Graphic